Electron spectra in the ionization of atoms by neutrinos

G. J. Gounaris,[1] E. A. Paschos,[2] and P. I. Porfyriadis[1]

[1]*Department of Theoretical Physics, Aristotle University of Thessaloniki, GR-54006 Thessaloniki, Greece*

[2]*Institut für Physik, Universität Dortmund, D-44221 Dortmund, Germany*

(Received 9 September 2004; published 9 December 2004)

For neutrinos of $\mathcal{O}(10\,\mathrm{keV})$ energies, their oscillation lengths are less than a few hundred meters, thereby suggesting the fascinating idea of oscillation experiments of small geometrical size. To help in evaluating this idea, a formalism is developed for calculating the neutrino ionization cross sections for H as well as the noble atoms. This formalism is based on the use of spin-independent atomic wave functions and should very accurately describe the ionization spectra for H, He, Ne, and Ar. The accuracy is considerably reduced for the Xe case though, where the spin dependence in the wave functions is non-negligible. Nevertheless, even for Xe the results remain qualitatively correct. In all cases, the atomic ionizations cross section per electron is found to be smaller than the neutrino cross section off free electrons, approaching it from below as the energy increases to the 100 keV region. At the 10–20 keV range though, the atomic binding effects in the cross sections and the spectra are very important and increasing with the atomic number. They are canceling out though, when total ionization cross section ratios, like ν_μ/ν_e or $\bar{\nu}_\mu/\bar{\nu}_e$, are considered.

DOI: 10.1103/PhysRevD.70.113008 PACS numbers: 13.15.+g

I. INTRODUCTION

Neutrino interactions have been observed and analyzed at energies from a few MeV (in reactor and solar neutrino experiments) [1], to several hundred GeV at accelerators. The lower keV energy range though has not attracted much interest up to now, due to the smaller cross sections there.

Nevertheless, when intense neutrino fluxes from radioactive decays become available, the possibility of very interesting experiments may arise, such as the testing of the solar neutrino oscillations using terrestrial experiments of rather small geometrical size [2]. To see this, we remark that recent results from the KamLAND experiment gives [3]

$$\Delta m^2_{12} = 8.2^{+0.3}_{-0.3} \times 10^{-5}\ \mathrm{eV}^2, \qquad \tan^2\theta_{12} = 0.39^{+0.09}_{-0.07}, \tag{1}$$

which would suggest a corresponding neutrino oscillation length of about 15 m for 1 keV neutrinos, increasing to 150 m when the energy reaches the 10 keV level. The oscillation length associated to $\Delta m^2_{13} \simeq \Delta m^2_{23}$ is about 27 times smaller [4].

To perform oscillation measurements at keV energies, the ionization of atoms by neutrinos may be used, taking of course into account the binding of the electrons. As an example we mention that the realization of an intense tritium source may allow the study of $\bar{\nu}_e$ oscillations in a room size experiment.

Such experiments may also help in investigating the weak interaction couplings at very low energies [2], the measuring of $\sin^2\theta_{13}$ [5], the search for measurable contributions from a neutrino magnetic moment [2,6,7], or contributions from possible new gauge bosons [8]. These are interesting questions, which were never investigated at very low energies, and may provide useful additional information on neutrino physics.

On the theoretical side, there are three calculations known to us investigating such effects. In [6], the energy spectrum of electrons knocked out from $^{19}\mathrm{F}(Z = 9)$ and $^{96}\mathrm{Mo}(Z = 42)$ atoms is computed, using relativistic electron wave functions. It is found that the electron ionization spectra differ significantly and are always smaller than those of the free scattering case.

In [9], we have also computed the total cross section on free electrons, as well as on bound electrons in some light atoms. At that time we studied the three atoms H, He, and Ne. The result again was that the ionization cross section per electron is always smaller than the cross section from free electrons [9], and never larger [10]. Moreover, this ionization cross section always decreases as we proceed from H to He to Ne, obviously due to the increase of the binding [9].

For planning and carrying out these new experiments though, it is needed to have the energy distribution of the ionization electrons for the noble gases He, Ne, and possibly Ar. The reason is that the detector sensitivity may generally depend on the ionization electron energy and it anyway diminishes below a certain limit; say, e.g., $\sim$10 eV [2]. In principle, Xe could also be useful, but such an experiment would be much more expensive than a Ne or Ar one [5]. Finally, the use of Kr is hindered, by the existence of a β^--emitting isotope [5].

The aim of the present paper is to present a method for calculating such spectra. We restrict to cases where it is adequate to consider the very accurate spin-independent atomic wave functions of [11]. This way, the most interesting cases of the He, Ne, and Ar atoms are covered, for which the results should be quite precise.

 © 2004 The American Physical Society

In principle our method could be extended to Xe, for which spin-independent wave functions are also given in [11]. But the results would then be less accurate.[1] This is suggested by the observation of a considerable spin dependence in the measured Xe binding energies [12], indicating that a dedicated relativistic treatment is needed for it. Thus only a very brief discussion of the integrated Xe ionization cross section is offered here.

Finally, since the properties of the detectors needed to experimentally study these ionization spectra are intensively investigated at present [2,5,13], the feasibility of this task is conveniently left outside the scope of the present work.

At the very low energies we are interested in, the standard model dynamics described by the diagrams in Fig. 1 induce the effective interaction Lagrangian

$$\mathcal{L}_{e\nu} = -\frac{G_F}{\sqrt{2}}\left\{\left[\bar{\nu}_e\gamma^\rho\frac{(1-\gamma_5)}{2}\nu_e\right][\upsilon_e\bar{e}\gamma_\rho e - a_e\bar{e}\gamma_\rho\gamma_5 e] + \left[\bar{\nu}_\mu\gamma^\rho\frac{(1-\gamma_5)}{2}\nu_\mu + \bar{\nu}_\tau\gamma^\rho\frac{(1-\gamma_5)}{2}\nu_\tau\right] \times [\tilde{\upsilon}_e\bar{e}\gamma_\rho e - \tilde{a}_e\bar{e}\gamma_\rho\gamma_5 e]\right\}, \quad (2)$$

describing the electron interactions with any neutrino flavor. The ν_e and (ν_μ, ν_τ) couplings are, respectively, given by

$$\upsilon_e = 1 + 4s_W^2, \qquad a_e = 1, \qquad \tilde{\upsilon}_e = -1 + 4s_W^2, \qquad \tilde{a}_e = -1, \quad (3)$$

while G_F is the usual Fermi coupling.

We first concentrate on the $\nu_e(\bar{\nu}_e)$ cases. From (2), the squared invariant amplitude $|F|^2$, summed over all initial and final electron spin states for the process

$$\nu_e(P_1)e^-(P_2) \to \nu_e(P_3)e^-(P_4) \quad (4)$$

is calculated, with the four-momenta being indicated in parentheses. The various particle energies are denoted below by E_j, and the standard variables,

$$s = (P_1 + P_2)^2 > m_e^2, \qquad t = (P_1 - P_3)^2, \qquad u = (P_1 - P_4)^2, \quad (5)$$

are used. We note that (4) describes the ν_e scattering from either a free or bound electron, the difference being determined by E_2, and, of course, the folded in momentum-wave function in the bound electron case.

Neglecting neutrino masses, we start from the case where the initial electron is free, so that $P_1^2 = P_3^2 = 0$, $P_2^2 = P_4^2 = m_e^2$, with m_e being the electron mass. Summing over all initial and final electron spin states, we then have

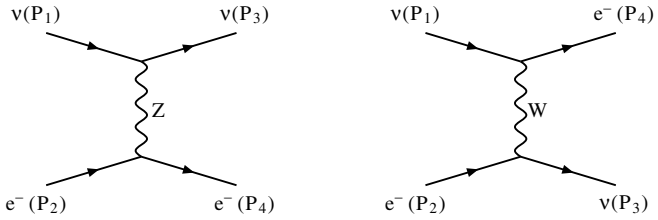

FIG. 1. The Feynman diagrams for $\nu_e e^-$ scattering.

$$|F(\nu_e e^- \to \nu_e e^-)|^2_{\text{free}} = 2G_F^2\{(\upsilon_e + a_e)^2(s - m_e^2)^2 + (\upsilon_e - a_e)^2(u - m_e^2)^2 + 2m_e^2(\upsilon_e^2 - a_e^2)t\}. \quad (6)$$

Because of crossing, the corresponding $|F|^2$ expression for the $\bar{\nu}_e$ case is simply obtained from the ν_e result, by interchanging $s \leftrightarrow u$ in (6).

In the lab system where the initial electron is at rest ($E_2 = m_e$), the differential cross section describing the energy distribution of the final electron is[2]

$$\left.\frac{d\sigma(\nu_e e^- \to \nu_e e^-)}{dE_4}\right|_{\text{free}} = \frac{m_e G_F^2}{8\pi E_1^2}\{(\upsilon_e + a_e)^2E_1^2 + (\upsilon_e - a_e)^2(E_1 + m_e - E_4)^2 + m_e(\upsilon_e^2 - a_e^2)(m_e - E_4)\}, \quad (7)$$

which, after it is integrated over the allowed range

$$m_e \le E_4 \le m_e + \frac{2E_1^2}{m_e + 2E_1}, \quad (8)$$

leads to the ν_e total cross section off free electrons

$$\sigma^{\nu e}_{\text{free}} \equiv \sigma(\nu_e e^- \to \nu_e e^-)|_{\text{free}} = \frac{m_e G_F^2 E_1}{8\pi} \times \left\{(\upsilon_e + a_e)^2\frac{2E_1}{m_e + 2E_1} + \frac{1}{3}(\upsilon_e - a_e)^2 \times \left[1 - \frac{m_e^3}{(m_e + 2E_1)^3}\right] - (\upsilon_e^2 - a_e^2)\frac{2m_e E_1}{(m_e + 2E_1)^2}\right\}. \quad (9)$$

Starting from (7), we present in[3] Fig. 2 the energy distribution of the final electrons, in ν_e and $\bar{\nu}_e$ scattering off free initial e^-. In these figures $E_e \equiv E_4$ is the final electron energy, and E_ν ($E_{\bar{\nu}}$) denote the incoming neutrino (antineutrino) energy E_1. As seen there, the energy distribution always has maximum at small E_e, which is also seen in all $\nu_e(\bar{\nu}_e)$-induced ionization cases; see below.

In Sec. II the formalism describing the ionization of atoms through neutrino (antineutrino) scattering is presented. This is done first for the hydrogen atom, and it is

[1] For an estimate of their error, see the discussion at the end of Sec. II.

[2] Notice that the laboratory angle of the emitted electron is not an independent variable, but is fixed completely by its energy.

[3] We always use $s_W^2 = 0.2312$.

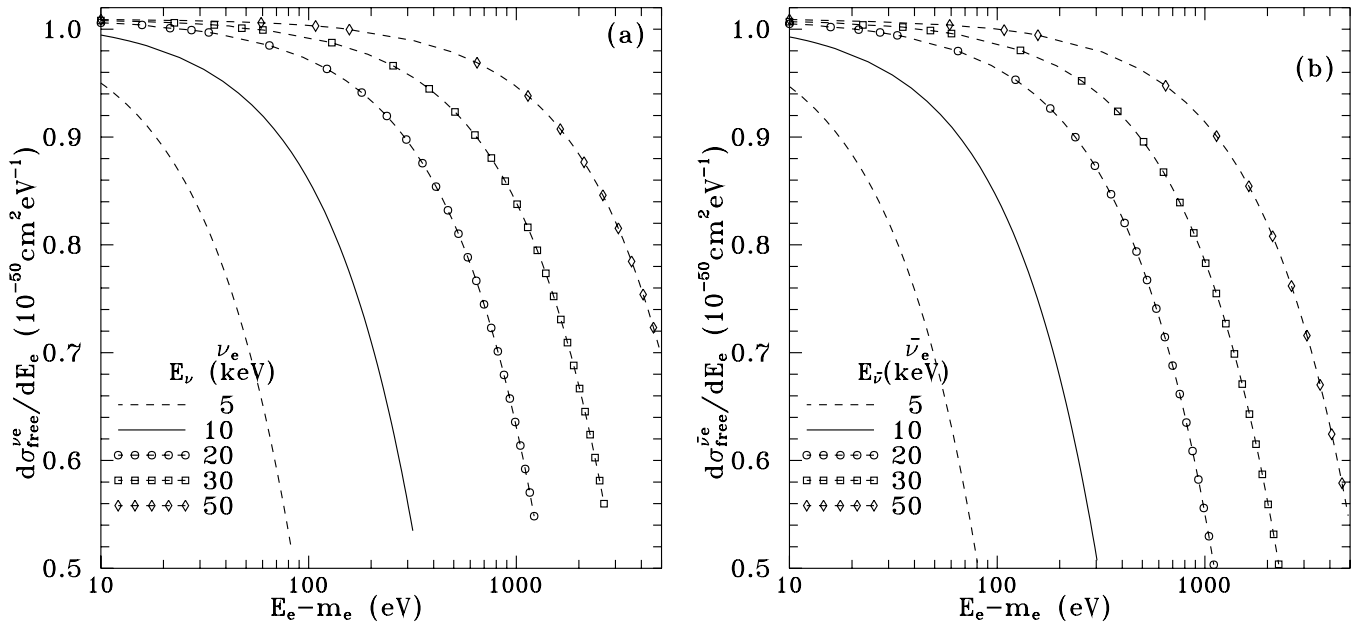

FIG. 2. The energy distribution of the final electron in $\nu_e e^-$ (a) or $\bar{\nu}_e e^-$ (b) scattering, at the rest frame of a free initial e^-. Here $E_e \equiv E_4$ is the final electron energy, and E_ν ($E_{\bar{\nu}}$) denotes the incoming neutrino (antineutrino) energy E_1; see text.

subsequently generalized to any atom characterized by complete electronic shells. A discussion of the accuracy of our method for the He, Ne, Ar, and Xe atoms is also given.

In Sec. III, we present the results for the energy distributions of the knocked out ionization electron in $\nu_e(\bar{\nu}_e)$ scattering for H, as well as for He, and Ne, using the analytic spin-independent Roothann-Hartree-Fock (RHF) wave functions published in [11]. In addition, we also present results for Ne ionization through ν_μ or ν_τ scattering, which might be generated through ν_e oscillation. Results for the integrated cross sections are also given in the same Sec. III, where we also include our predictions for the Xe case. The conclusions are presented in Sec. IV. Important details on the kinematics and atomic wave functions are relegated to Appendixes A and B, respectively.

II. THE FORMALISM

The ionization of atoms through neutrino scattering off atomic electrons requires from atomic physics the electron binding energy and the wave functions in momentum space. The energy of the initial bound electron is fixed by the binding energy ϵ, so that

$$E_2 = m_e + \epsilon, \tag{10}$$

with ϵ being negative. For the simplest H atom, ϵ is fixed by the Balmer formula, while for more complicated atoms, we use the experimental measurements [12].

The three-dimensional momentum of the bound electron however [compare definitions in (A1)] varies according to the probability distribution

$$|\tilde{\Psi}_{nlm}(p_2, \theta_2, \phi_2)|^2 \frac{p_2^2 dp_2 d\cos\theta_2 d\phi_2}{(2\pi)^3}, \tag{11}$$

determined by the momentum-wave function[4] $\tilde{\Psi}_{nlm}(p_2, \theta_2, \phi_2)$, when electron spin effects are neglected. Therefore, the bound electron may get off shell with an effective squared mass given by

$$\tilde{m}^2 \equiv P_2^2 = E_2^2 - p_2^2, \tag{12}$$

so that the standard kinematical variables defined in (5) satisfy

$$s + t + u = \tilde{m}^2 + m_e^2. \tag{13}$$

The squared invariant amplitude for the ν_e-electron subprocess, summed over all initial and final electron spin states,[5] is written as [9]

$$\begin{aligned}|F(\nu_e e^- \to \nu_e e^-)|^2 = 2G_F^2\{&(v_e + a_e)^2(s - m_e^2)(s - \tilde{m}^2) \\ &+ (v_e - a_e)^2(u - m_e^2)(u - \tilde{m}^2) \\ &+ 2m_e^2(v_e^2 - a_e^2)t\},\end{aligned} \tag{14}$$

which of course becomes identical to (6) when $\tilde{m}^2 \to m_e^2$. As in the free electron case, the antineutrino result may be obtained from (14) by interchanging $s \leftrightarrow u$.

[4]The momentum here is connected to the wave function determining the probability distribution. It is the conjugate variable to the position coordinates and provides the Fourier transform of the wave function; see Appendix B.

[5]Justified because we neglect any spin dependence on the wave function.

For clarity, we first consider the ionization of a hydrogen atom being initially in its ground state. The energy spectrum of the ionized electron is obtained by averaging over the bound electron momenta according to its wave function [see Eqs. (15) of [9]], and subsequently changing the $d\sigma/du$ distribution to $d\sigma/dE_4$, which brings in the derivative du/dE_4. We thus get

$$\frac{d\sigma_{\mathrm{H}}^{\nu e}}{dE_4} = \frac{1}{64\pi E_1 E_2} \times \int \frac{d\phi_2 d\cos\theta_2 p_2^2 dp_2}{(2\pi)^3 (s-\tilde{m}^2)} |\tilde{\Psi}_{100}(p_2)|^2 |F|^2 \left| \frac{du}{dE_4} \right|. \tag{15}$$

The variables (p_2, θ_2, ϕ_2) are the momentum and angles of the bound electron in the rest frame of the atom [compare (A1)]; and[6] $\tilde{\Psi}_{100}(p_2)$ is the ground state momentum-wave function defined in (B5). Finally E_2 is determined through (10), which for the H ground state $(n = 1, l = 0)$ is given by

$$\epsilon = \epsilon_{1s}^{\mathrm{H}} = -\frac{m_e \alpha^2}{2} = -13.6 \text{ eV}. \tag{16}$$

The kinematics are fully explained in Appendix A; compare (4). According to it, for any (θ_2, ϕ_2) in the range (A3), and any value of the bound electron's momentum p_2 and the incoming neutrino energy E_1, the polar angle of the ionization electron θ_4 is a function of its energy E_4 given by[7] (A6). This function is used to determine through (A9), the expression for du/dE_4 needed in (15).

We also note that the angular dependence of the integrant in (15) is only due to (A9) and the effect of (A4) on $|F|^2$. The angular integration is done numerically, with its range fixed by (A3). For the numerical evaluation of the p_2 integral, the relevant part of the p_2 range is determined by the form of the electron wave function, as discussed immediately after (B5) and at the end of Appendix B.

We next turn to the general case of any of the noble gas atoms He, Ne, Ar, Kr, and Xe. Their wave functions are discussed in Appendix B [11]. Since for noble atoms all electronic shells are complete, a summation of the form

$$\sum_{m=-l}^{l} |Y_{lm}|^2 = \frac{2l+1}{4\pi}$$

always appears in the wave function contribution to ionization, washing out any angular dependence from it. As a result, the energy distribution of the ionization electron for any noble atom, normalized to one electron per unit volume, may be obtained from (15) by replacing

$$|\tilde{\Psi}_{100}(p_2)|^2 \to \frac{1}{Z\cdot 4\pi}\{2[\tilde{R}_{10}(p_2)]^2 + 2[\tilde{R}_{20}(p_2)]^2 + 6[\tilde{R}_{21}(p_2)]^2 + 2[\tilde{R}_{30}(p_2)]^2 + 6[\tilde{R}_{31}(p_2)]^2 + 10[\tilde{R}_{32}(p_2)]^2 + 2[\tilde{R}_{40}(p_2)]^2 + 6[\tilde{R}_{41}(p_2)]^2 + 10[\tilde{R}_{42}(p_2)]^2 + 2[\tilde{R}_{50}(p_2)]^2 + 6[\tilde{R}_{51}(p_2)]^2\}, \tag{17}$$

where $\tilde{R}_{nl}(p_2)$ are the radial momentum-wave functions defined in (B2), and Z is the atomic number.

Focusing to the expression within the curly brackets on the right-hand side (r.h.s.) of (17), we remark that by restricting to just the first (one, three, five, eight, all) terms, we obtain, respectively, the results for the (He, Ne, Ar, Kr, Xe) atoms, provided the appropriate Z value is used. The corresponding atomic wave functions are discussed in Appendix B and [11].

We next turn to the discussion of the reliability of our calculation. We first recall that a very high accuracy of more than eight digits has been claimed by the authors of [11], for all RHF (spin averaged) energies of their results, for all atoms from[8] He to Xe. The main weakness comes therefore from the neglect of spin effects in the atomic wave functions. This should be no problem for the lighter atoms up to Kr, for which the experimental data on the electron binding energies indicate that the spin effects are smaller than $\sim 1\%$ [12]. Therefore, our results for He and Ne, and those that could be obtained by applying our procedure to Ar and Kr, should be accurate at the 2% level, their main error coming from electromagnetic radiative corrections and small relativistic spin effects.

For Xe though, the spin dependence of the electron binding energies shown in Table I is more significant, suggesting that the error in the individual ionization cross

TABLE I. Relative spin effect in the binding energies of the various electronic quantum states in Xe [12].

Quantum states	Spin effect
$2p_{1/2} - 2p_{3/2}$	6.6%
$3p_{1/2} - 3p_{3/2}$	6.4%
$3d_{3/2} - 3d_{5/2}$	1.8%
$4p_{1/2} - 4p_{3/2}$	0.8%
$4d_{3/2} - 4d_{5/2}$	2.9%
$5p_{1/2} - 5p_{3/2}$	10.4%

[6]This wave function has no angular dependence, because of the vanishing of the orbital angular momentum.

[7]See the discussion immediately after (A6) for resolving any ambiguity.

[8]See in particular the last sentences in Appendix B quoted from their paper.

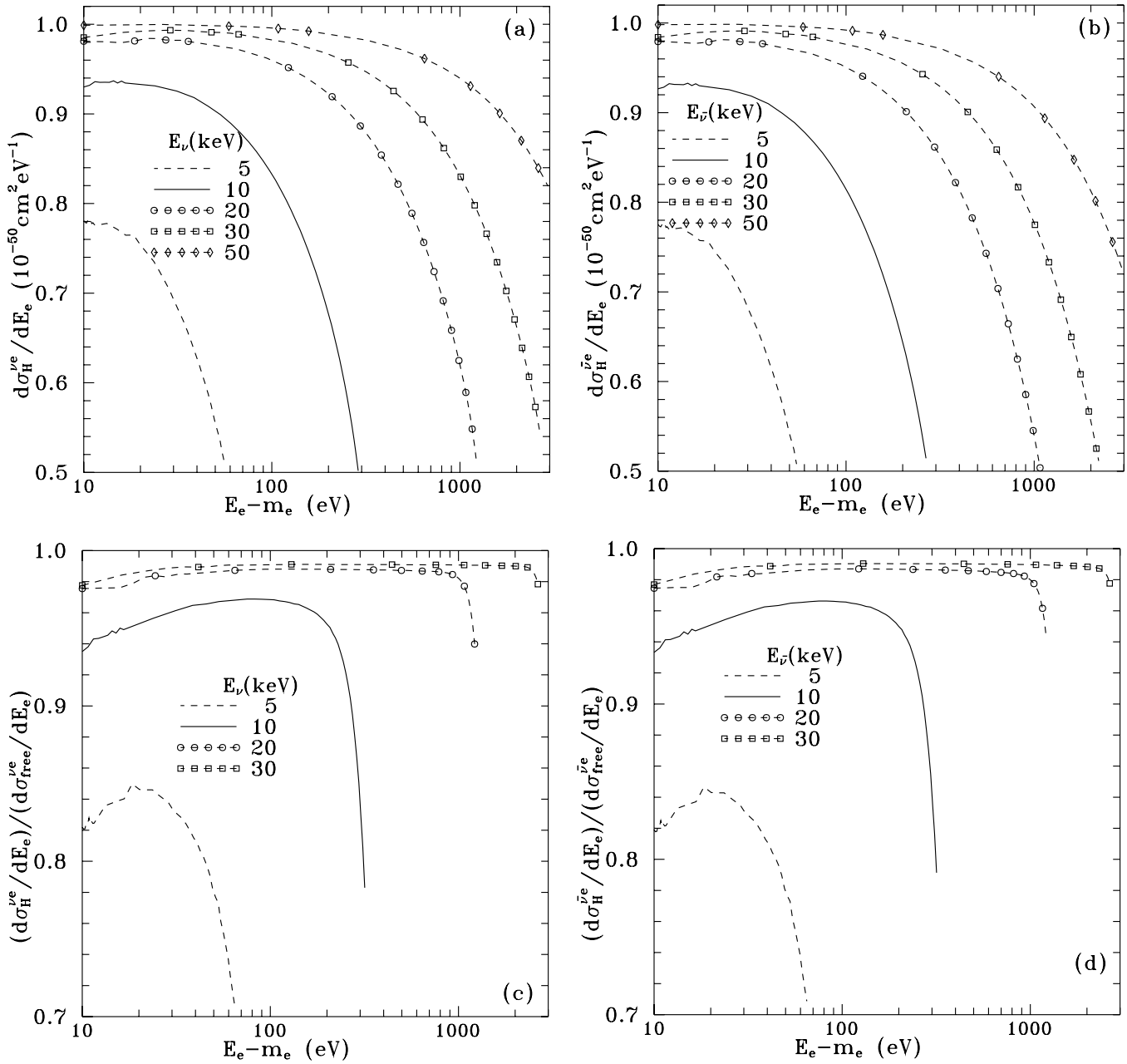

FIG. 3. The electron energy distribution in ν_e (a) or $\bar{\nu}_e$ (b) ionization of H, and their respective ratios (c) and (d) to the corresponding distributions when the initial electron is assumed as free. Variables defined as in caption of Fig. 2.

section could possibly reach the 10% level.[9] In the discussion of Sec. III we find indications though that this error is in fact diminished in the ratio of the ν_μ/ν_e total cross sections determining θ_{13}. The electron binding effect seems canceling in this ratio.

[9]Note that the stronger singularity of the relativistic wave functions at small distances, which increases the momentum-wave functions at large momenta, should have no effect on the ionizations, since in this range the wave functions are strongly suppressed.

III. RESULTS FOR NEUTRINO IONIZATION OF ATOMS

Using (15) and (16) and the H-wave function in (B5), we obtain the results in Fig. 3 describing the energy distributions of the knocked out electron in $\nu_e(\bar{\nu}_e)$ ionization of hydrogen, normalized to one electron per unit volume. The results apply to various incoming neutrino energies.

The corresponding distributions for He and Ne atoms are shown in Figs. 4 and 5 respectively, using the wave functions of Appendix B and the parameters tabulated in [11]. For the electron binding energies in the various atoms

(including those of Xe we discuss below), we use the experimental values [12]

$$\text{He: } \epsilon_{1s}^{\text{He}} = -24.6 \text{ eV}, \tag{18}$$

$$\text{Ne: } \epsilon_{1s}^{\text{Ne}} = -870.2 \text{ eV}, \quad \epsilon_{2s}^{\text{Ne}} = -48.5 \text{ eV}, \quad \epsilon_{2p}^{\text{Ne}} = -21.7 \text{ eV}, \tag{19}$$

$$\begin{aligned} \text{Xe: } &\epsilon_{1s}^{\text{Xe}} = -34\,561 \text{ eV}, \quad \epsilon_{2s}^{\text{Xe}} = -5453 \text{ eV}, \quad \epsilon_{2p}^{\text{Xe}} = -4893 \text{ eV}, \quad \epsilon_{3s}^{\text{Xe}} = -1149 \text{ eV}, \\ &\epsilon_{3p}^{\text{Xe}} = -961 \text{ eV}, \quad \epsilon_{3d}^{\text{Xe}} = -681.4 \text{ eV}, \quad \epsilon_{4s}^{\text{Xe}} = -213.2 \text{ eV}, \quad \epsilon_{4p}^{\text{Xe}} = -145.7 \text{ eV}, \\ &\epsilon_{4d}^{\text{Xe}} = -68.3 \text{ eV}, \quad \epsilon_{5s}^{\text{Xe}} = -23.3 \text{ eV}, \quad \epsilon_{5p}^{\text{Xe}} = -12.5 \text{ eV}. \end{aligned} \tag{20}$$

As seen from Figs. 2–5 the energy distribution in all $\nu_e(\bar{\nu}_e)$-induced cross sections is maximal at small $E_e = E_4$.

Concerning Figs. 3–5 we may remark that for E_1 in the few 10 keV range, the differential $d\sigma/dE_4$ ionization cross sections per electron are always at the level of 10^{-50} cm^2 eV^{-1}. Moreover, they are always smaller than the ''free electron'' ones, approaching them from below as E_1 increases; see the (c) and (d) parts of each of these figures. For a fixed E_1 value though, $d\sigma/dE_4$ always decreases as we go from hydrogen to Ne and then to xenon.

The integrated $\nu_e(\bar{\nu}_e)$-ionization cross sections for final electron energies $E_4 > m_e + 10$ eV, are shown in Fig. 6. Here again the cross sections are normalized to one electron per unit volume. In the same figure the corresponding integrated cross section off free electrons are also included, as well as our predictions for Xe. As seen from Figs. 6(a) and 6(b) all cross sections are of the order of 10^{-47} cm^2 at $E_1 \sim 15$ keV, increasing with the neutrino energy. The ratios of the integrated ionization cross sections to the free electron one are shown in Figs. 6(c) and 6(d). As expected, the integrated ionization cross section is also always smaller than the free one, approaching it from below. For H and He the approach is very fast, but it becomes much slower for heavier atoms; see, e.g., the results for Ne and Xe. Thus at $E_1 \sim 50$ keV the Ne cross section is still about 5% smaller than the free e one, while for Xe the decrease is at the $\sim$30% level.

Such integrated ionization cross sections for H, He, and Ne have already appeared in [9]. The present results are consistent with those. We should point out though that in [9], the integrated cross sections were calculated over the entire physical region $E_4 > m_e$. Moreover, in that work we had used a very rough approximation for the He wave function based on the Z_{eff} idea, while the Ne results were based on the old fit of Tubis [14]. Thus although the present results are consistent with those of [9], prospective users should rely more on the present ones based on [11]. After all, it is only here that the energy distribution of the ionization electron appears.

We have already estimated that for ν_e or $\bar{\nu}_e$ in the 10 keV level, the oscillation length is about 150 m; see (1). Consequently, the other neutrino flavors should also be generated, as the initial ν_e or $\bar{\nu}_e$ proceeds in a volume filed with a noble gas. Thus, in a tritium decay experiment, $\bar{\nu}_\mu$ and $\bar{\nu}_\tau$ should appear in relative amounts determined by the mixing angles and the distance from the source.

The treatment of the ν_μ effects is exactly the same as for ν_e, the only difference being that in (6) and (14) we now have to use the second set of the neutrino vector and axial couplings listed in (3); compare (2). The resulting differential cross section for scattering off a free electron is then given in Fig. 7, which is strikingly different from the corresponding $\nu_e(\bar{\nu}_e)$ result shown in Fig. 2. A similar situation arises also for Ne ionization; compare the ν_μ induced ionization shown in Fig. 8 to the corresponding ν_e effect in Fig. 5. Again, the E_e distributions tend to have a local minimum at low final electron energies in Figs. 7 and 8, in contrast to the local maximum in Figs. 2–5.

We have moreover found that for neutrinos (antineutrinos) at the 10–20 keV range, the respective ratio of their integrated cross sections[10] ν_μ/ν_e ($\bar{\nu}_\mu/\bar{\nu}_e$) remains almost constant and equal to 0.42 (0.44), as we move from the free electron case, to the Ne and the Xe ionization ones. This suggests that all binding effects in the individual ν_e and ν_μ integrated cross sections are canceling in their ratio, for which the simple expression (9) is adequate.

It is worth remarking also on the basis of Figs. 7 and 8 that the ν_μ and $\bar{\nu}_\mu$ results are almost identical. This is due to the fact that $\tilde{v}_e \simeq 0$, for the value of the Weinberg angle we use [compare (3)], which makes the squared amplitudes in (6) and (14) almost $s \leftrightarrow u$ symmetric. It seems therefore that a tritium experiment may also give information on the value of the Weinberg angle at the keV scale [13]. The ν_τ results are of course identical to those for ν_μ; compare (2).

We next briefly address the problem of the flavor oscillation of the neutrino induced noble gas ionization. Since for reasonable gas densities the vacuum oscillation treatment should be adequate, the oscillation probabilities may be written as

$$P(\nu_e \to \nu_\mu + \nu_\tau) = \sin^2(2\theta_{12})\cos^4(\theta_{13})\sin^2\left(\frac{\Delta_{12}L}{4E_1}\right) + \sin^2(2\theta_{13})\sin^2\left(\frac{\Delta_{13}L}{4E_1}\right), \tag{21}$$

[10]Integrated for $E_e - m_e > 10$ eV.

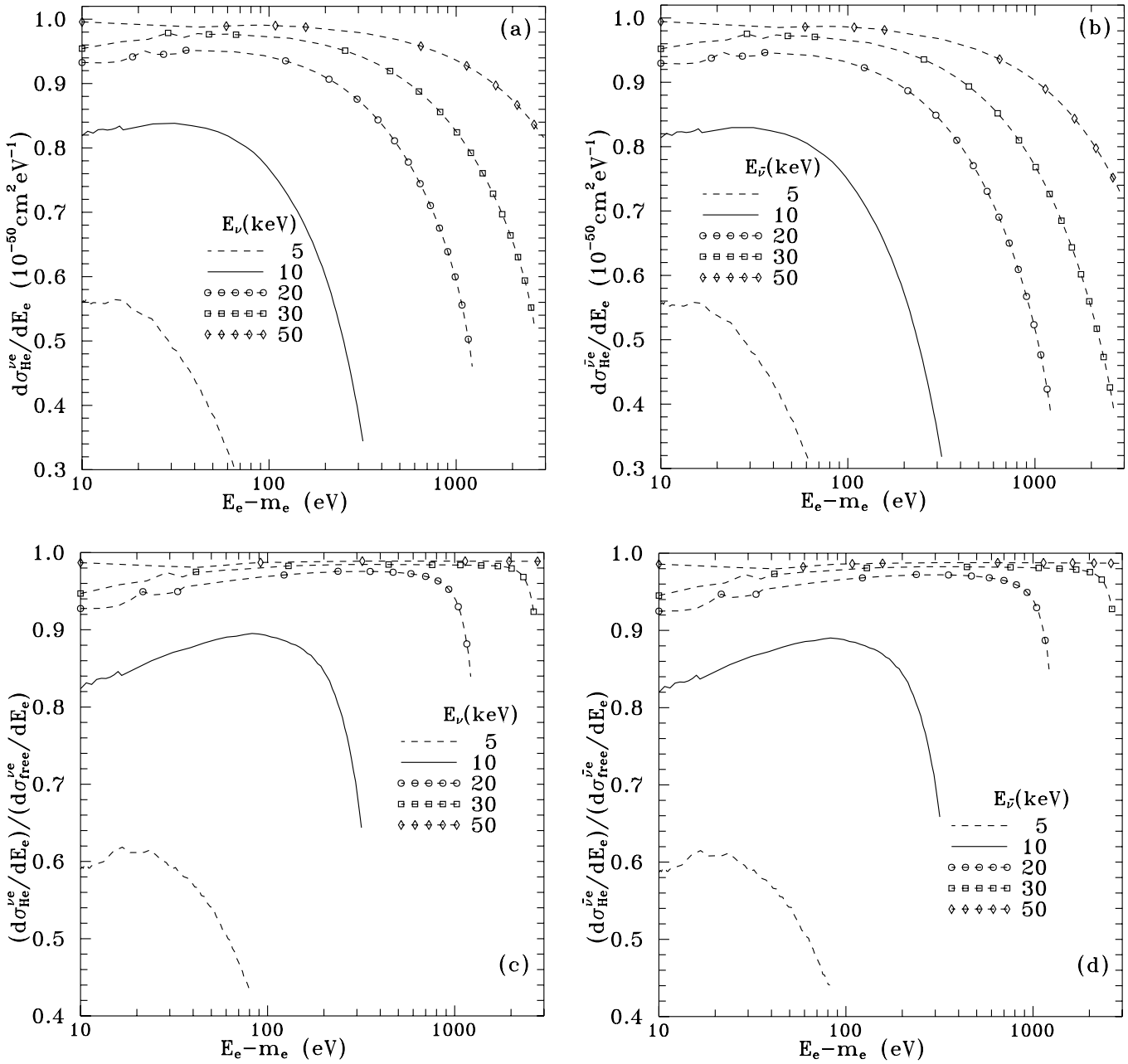

FIG. 4. The electron energy distribution in ν_e (a) or $\bar{\nu}_e$ (b) ionization of He normalized to one e^- per unit volume, and their respective ratios (c) and (d) to the corresponding distributions when the initial electron is assumed as free; see Fig. 2. Variables defined as in caption of Fig. 2.

$$P(\nu_e \to \nu_e) = 1 - P(\nu_e \to \nu_\mu + \nu_\tau), \qquad (22)$$

assuming three active and no sterile neutrinos. Here θ_{12}, θ_{23}, and θ_{13} are the three mixing angles, while $\Delta_{ij} \equiv m_j^2 - m_i^2$ denote the mass differences between the neutrino masses satisfying $|\Delta_{13}| \simeq |\Delta_{23}| \gg |\Delta_{12}|$ [1,4], and L is the distance from the source. We note that there is no dependence on the neutrino CP-violating phase δ in (21) and (22), and that these same formulas describe antineutrino oscillations also.

Thus, as an initially produced ν_e transverses, e.g., a Ne target, the ionization cross section per electron varies with L as

$$\frac{d\sigma_{\rm Ne}}{dE_4} = [1 - P(\nu_e \to \nu_\mu + \nu_\tau)] \cdot \frac{d\sigma^{\nu e}_{\rm Ne}}{dE_4}\bigg|_{\nu=\nu_e} + P(\nu_e \to \nu_\mu + \nu_\tau) \cdot \frac{d\sigma^{\nu e}_{\rm Ne}}{dE_4}\bigg|_{\nu=\nu_\mu}, \qquad (23)$$

in the r.h.s. of which (15) and (17) should be used for

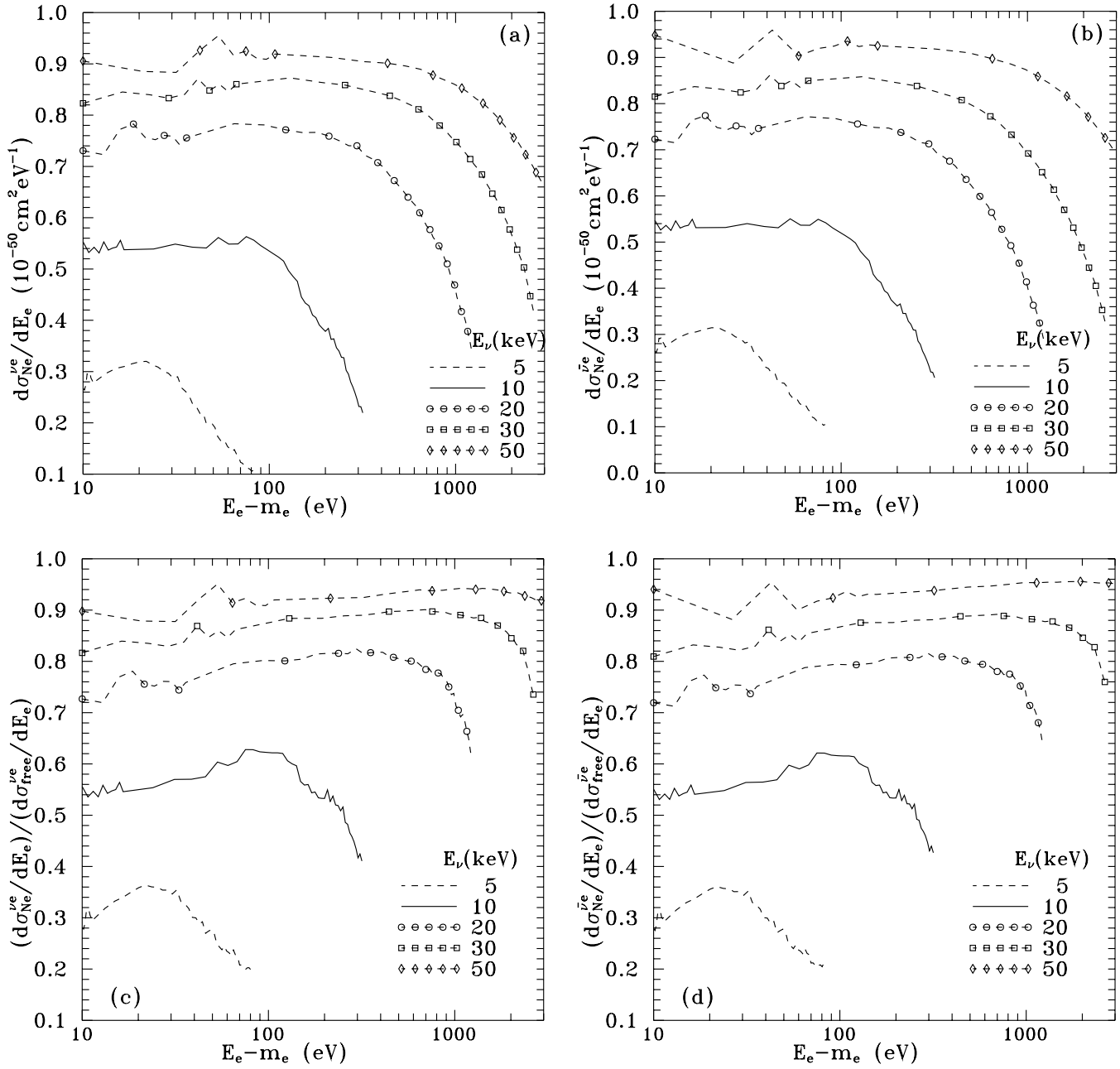

FIG. 5. The electron energy distribution in ν_e (a) or $\bar{\nu}_e$ (b) ionization of Ne normalized to one e^- per unit volume, and their respective ratios (c) and (d) to the corresponding distributions when the initial electron is assumed as free; see Fig. 2. Variables defined as in caption of Fig. 2.

$\nu = \nu_e$ and $\nu = \nu_\mu$ respectively. Correspondingly for antineutrinos.

Using the experimental Δ_{ij} values, we find that the oscillation length of the first term of $P(\nu_e \to \nu_\mu + \nu_\tau)$ [see (21)] is about 150 m for an incoming neutrino energy of $E_1 \simeq 10$ keV, while the oscillation length of the second term is only about 5.6 m. Since θ_{13} is known to be very small, the picture created by (23) will then consist of a few hundred meter oscillation, modulated by a much weaker one of a few meter size [4]. The strength of the modulation is determined only by θ_{13} and the ratio of the ν_μ to ν_e cross sections. As we have already stated, an enhancement of the theoretical accuracy of this ratio immediately implies also an increase to the θ_{13} sensitivity.

Depending, therefore, on the achievable experimental accuracy, the study $\bar{\nu}_e$ oscillations in tritium decay may help further constraining the neutrino mixing angles and masses. This would be most interesting for θ_{13}, for which

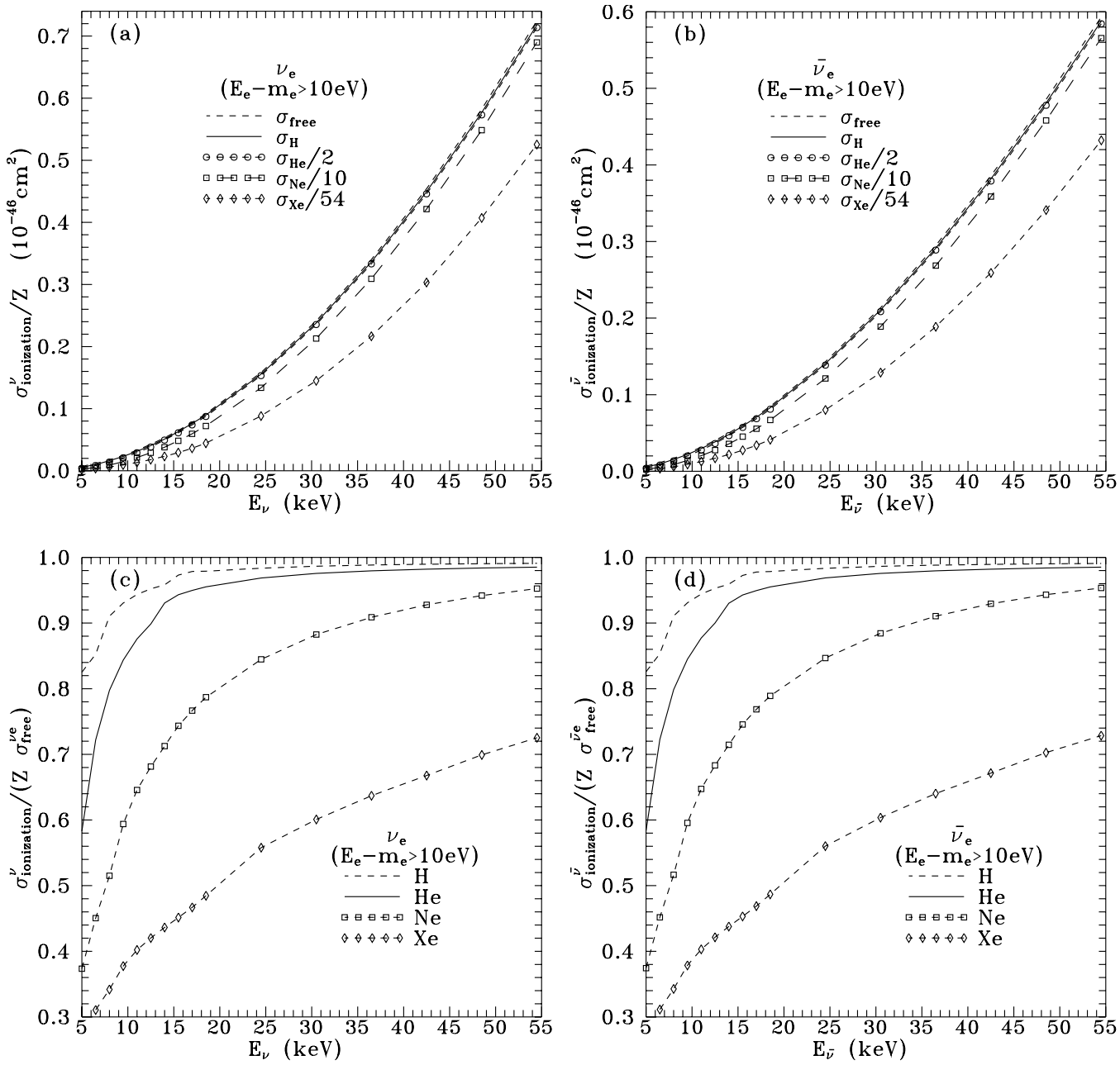

FIG. 6. The ν_e (a) [$\bar{\nu}_e$ (b)] ionization integrated cross sections for H, He, Ne, and Xe atoms divided by Z, and the cross section off free electrons at rest, as a function of the ν_e [$\bar{\nu}_e$] energy. The ratios of these ionization cross sections to the free electron ones are given in (c) and (d), respectively.

information might be derived if a future experiment manages to be sensitive to both oscillation lengths governing (21).

IV. CONCLUSIONS

In this paper we have presented a formalism for the ionization of atoms by bombarding them with neutrinos of any flavor in the keV energy range. The interest in this energy range originates from the fact that the oscillation lengths for neutrinos in the few keV range become rather small, allowing the possibility of studying the oscillations observed in the solar neutrino and KamLAND experiments, by means of a terrestrial experiment of small size. A highlight of such an experiment is to improve the constraint on θ_{13}. Neutrinos in this energy may be obtained from various possible beta decays, most notably tritium decay producing antineutrinos.

Motivated by this, we have undertaken the present extensive study of the ionization of H and the noble atoms by neutrinos. To this purpose, we have developed a method based on spin-independent atomic wave functions, for which we use the very accurate RHF wave functions listed

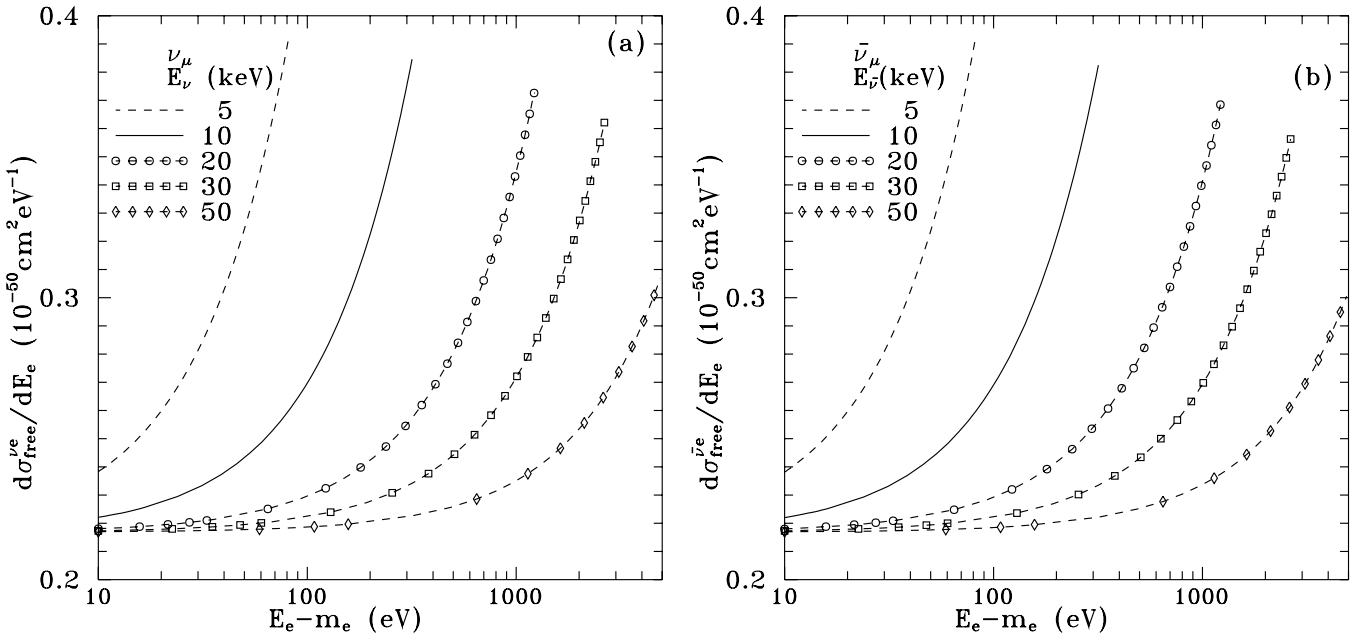

FIG. 7. The energy distribution of the final electron in $\nu_\mu e^-$ (a) or $\bar{\nu}_\mu e^-$ (b) scattering, at the rest frame of a free initial e^-. Here $E_e \equiv E_4$ is the final electron energy, and E_ν ($E_{\bar{\nu}}$) denotes the incoming neutrino (antineutrino) energy E_1. Identical results for ν_τ.

in [11]. The energy of the bound electron in each atomic state is fixed by its binding energy, while its momentum varies according to the distribution determined by the momentum-wave function, thereby generally forcing the electron to get off shell. The method is very accurate for treating H and the most interesting noble gases He, Ne, and Ar.

On the other hand, it is less accurate for Xe, where considerable spin dependence appears. Thus, for Xe we have simply given the results of the present method for the integrated ionization cross section, whose accuracy should be lying at the 10% level or so. This completes the overall view of the neutrino ionization of the noble gases. If the use of Xe in such an experiment is finally decided though, then of course a special treatment would be needed, based on spin depended atomic wave functions.

We next proceed to summarize our extensive results. We have found that at the 10–20 keV neutrino energy range, the differential cross sections $d\sigma/dE_e$ are at the 10^{-50} cm^2/eV level for $\nu_e(\bar{\nu}_e)$-induced processes, while the integrated cross section is of the order of 10^{-47} cm^2. At the 10–20 keV neutrino energy range, atomic effects are very important and cannot be ignored. They reduce the Ne ionization cross section per electron by almost 20%, while for Xe the reduction reaches the factor of 2 level. Of course, as the incoming neutrino energy increases beyond, e.g., the 100 keV region, all these ''per-electron'' ionization cross sections approach the neutrino cross section off free electrons, always from below.

We have also compared the ν_e induced reactions, with those induced by ν_μ or ν_τ, the latter two being equal to each other. The difference between the two comes from the fact that ν_e reactions involve both charged and neutral current diagrams, while for ν_μ, ν_τ only neutral currents contribute. As a result, the energy distribution of the final electron in the ν_μ reactions tends to have a local minimum at low electron energies, in contrast to the local maximum expected for the corresponding ν_e effect. Moreover for 10–20 keV neutrinos or antineutrinos, the ratio of their integrated cross sections is found to be largely independent of any atomic binding effects.

As an overall conclusion we may state that if such small cross sections become measurable one day, neutrino atomic ionization experiments may be useful for testing the electroweak theory at keV energies and studying the neutrino mixing.

ACKNOWLEDGMENTS

The support of the ''Bundesministerium für Bildung, Wissenschaft, Forschung und Technologie,'' Bonn under Contract No. 05HT1PEA9 and the support by the European Union under the RTN Contracts No. HPRN-CT-2000-00148 and No. MRTN-CT-2004-503369 is gratefully acknowledged. P. I. P. is also grateful to the Institut für Physik, Universität Dortmund, for the hospitality extended to him during part of this work.

APPENDIX A: KINEMATICS

In the rest frame of the atom, defining the $\hat{z}$ axis along the direction of the incoming neutrino and the xz plane as the plane where the (final) ionization electron lies, we write [compare (4)]

$$P_1^\mu = \begin{pmatrix} E_1 \\ 0 \\ 0 \\ E_1 \end{pmatrix}, \qquad P_2^\mu = \begin{pmatrix} E_2 \\ p_2 \sin\theta_2 \cos\phi_2 \\ p_2 \sin\theta_2 \sin\phi_2 \\ p_2 \cos\theta_2 \end{pmatrix},$$
$$P_4^\mu = \begin{pmatrix} E_4 \\ p_4 \sin\theta_4 \\ 0 \\ p_4 \cos\theta_4 \end{pmatrix}, \tag{A1}$$

where E_1 is the energy of the initial neutrino; $(E_2, p_2, \theta_2, \phi_2)$ are the energy, momentum, and angles of the electron bound inside the atom; and (E_4, p_4, θ_4) are the energy, momentum, and polar angle of the freely moving final ionization electron. By definition, the range of these angles is

$$0 < \theta_4 < \pi, \tag{A2}$$

$$0 < \theta_2 < \pi, \qquad 0 < \phi_2 < 2\pi. \tag{A3}$$

The standard variables defined in (5) become

$$\begin{aligned} s &= \tilde{m}^2 + 2E_1(E_2 - p_2\cos\theta_2), \\ t &= m_e^2 - 2E_1(E_4 - p_4\cos\theta_4), \\ u &= 2E_1(E_4 - p_4\cos\theta_4 - E_2 + p_2\cos\theta_2), \end{aligned} \tag{A4}$$

where the definition (12) is used, and (13) is of course satisfied.

The requirement of

$$P_3^2 = (P_1 + P_2 - P_4)^2 = 0 \tag{A5}$$

implied by the negligibly small neutrino mass leads to an equation determining $\cos\theta_4$ in terms of E_4 and E_1. In the free electron case, this is linear in $\cos\theta_4$, and it can be solved immediately leading to (7).

For bound electrons, however, (A5) leads to a quadratic equation in $\cos\theta_4$, which also depends on the momentum and spherical angles of the bound electron. It is then important to discriminate between the two mathematically possible solutions, among which only one is physically acceptable. To do this we first note that the general solution of (A5) may be written as

$$\tan\left(\frac{\theta_4}{2}\right) = \frac{\zeta_1 \pm \sqrt{\zeta_1^2 - \zeta_2}}{2\zeta_3}, \tag{A6}$$

where

$$\begin{aligned} \zeta_1 &= 2p_4 p_2 \sin\theta_2 \cos\phi_2, \\ \zeta_2 &= 4\{[E_4(E_1 + E_2) - \xi]^2 - p_4^2(E_1 + p_2\cos\theta_2)^2\}, \\ \zeta_3 &= E_4(E_1 + E_2) - \xi + p_4(E_1 + p_2\cos\theta_2), \end{aligned} \tag{A7}$$

$$\xi = -E_1 p_2 \cos\theta_2 + E_1 E_2 + \frac{m_e^2 + \tilde{m}^2}{2}. \tag{A8}$$

A detail study indicates that whenever both θ_4 solutions of (A6) satisfy (A2), the physically acceptable one is given by the upper (lower) sign of (A6), depending on whether[11] $\zeta_1 > 0$ ($\zeta_1 < 0$), respectively. This physically acceptable θ_4 solution is, by its very definition, a continuous function of the ionization electron energy and the bound electron's momentum and angles entering the integration in (15).

Once the physically acceptable θ_4 solution in (A6) has been identified, du/dE_4 entering (15) is determined from

$$\begin{aligned} \frac{du}{dE_4} &= -2E_1\left(1 - \frac{E_4}{p_4}\cos\theta_4 + p_4\frac{d\theta_4}{dE_4}\sin\theta_4\right), \\ \frac{d\theta_4}{dE_4} &= \frac{E_4[E_1\cos\theta_4 + p_2(\cos\theta_2\cos\theta_4 + \sin\theta_2\sin\theta_4\cos\phi_2)] - (E_1 + E_2)p_4}{p_4^2[E_1\sin\theta_4 + p_2(\cos\theta_2\sin\theta_4 - \sin\theta_2\cos\theta_4\cos\phi_2)]}. \end{aligned} \tag{A9}$$

Finally, the requirement $\zeta_1^2 \geq \zeta_2$ [note the square root in (A6)] implies that the range of E_4 is determined by

$$E_4^{(2)} \leq E_4 \leq E_4^{(1)}, \tag{A10}$$

with

$$E_4^{(1,2)} = \frac{\xi(E_1 + E_2) \pm \xi_1\sqrt{\xi^2 - m_e^2[(E_1 + E_2)^2 - \xi_1^2]}}{(E_1 + E_2)^2 - \xi_1^2}, \tag{A11}$$
$$\xi_1 = \sqrt{(E_1 + p_2\cos\theta_2)^2 + p_2^2\sin^2\theta_2\cos^2\phi_2}.$$

APPENDIX B: THE ATOMIC WAVE FUNCTIONS

The atomic wave functions in the momentum space needed in (15) are related to the coordinate wave functions by

$$\tilde{\Psi}_{nlm}(\vec{k}) = \int d^3r \Psi_{nlm}(\vec{r}) e^{-i\vec{k}\cdot\vec{r}}, \tag{B1}$$

where nlm denote the usual quantum numbers characterizing atomic states. The radial momentum-wave function defined by the first function on the r.h.s. of[12]

$$\tilde{\Psi}_{nlm}(\vec{k}) = (-i)^l \tilde{R}_{nl}(k) Y_{lm}(\hat{k}) \tag{B2}$$

is related to the radial wave function in coordinate space

[11] According to the first of (A7), this is equivalent to $\cos\phi_2$ being positive (negative), respectively.

[12] $Y_{lm}(\hat{k})$ is the usual spherical harmonic function depending on the momentum angles.

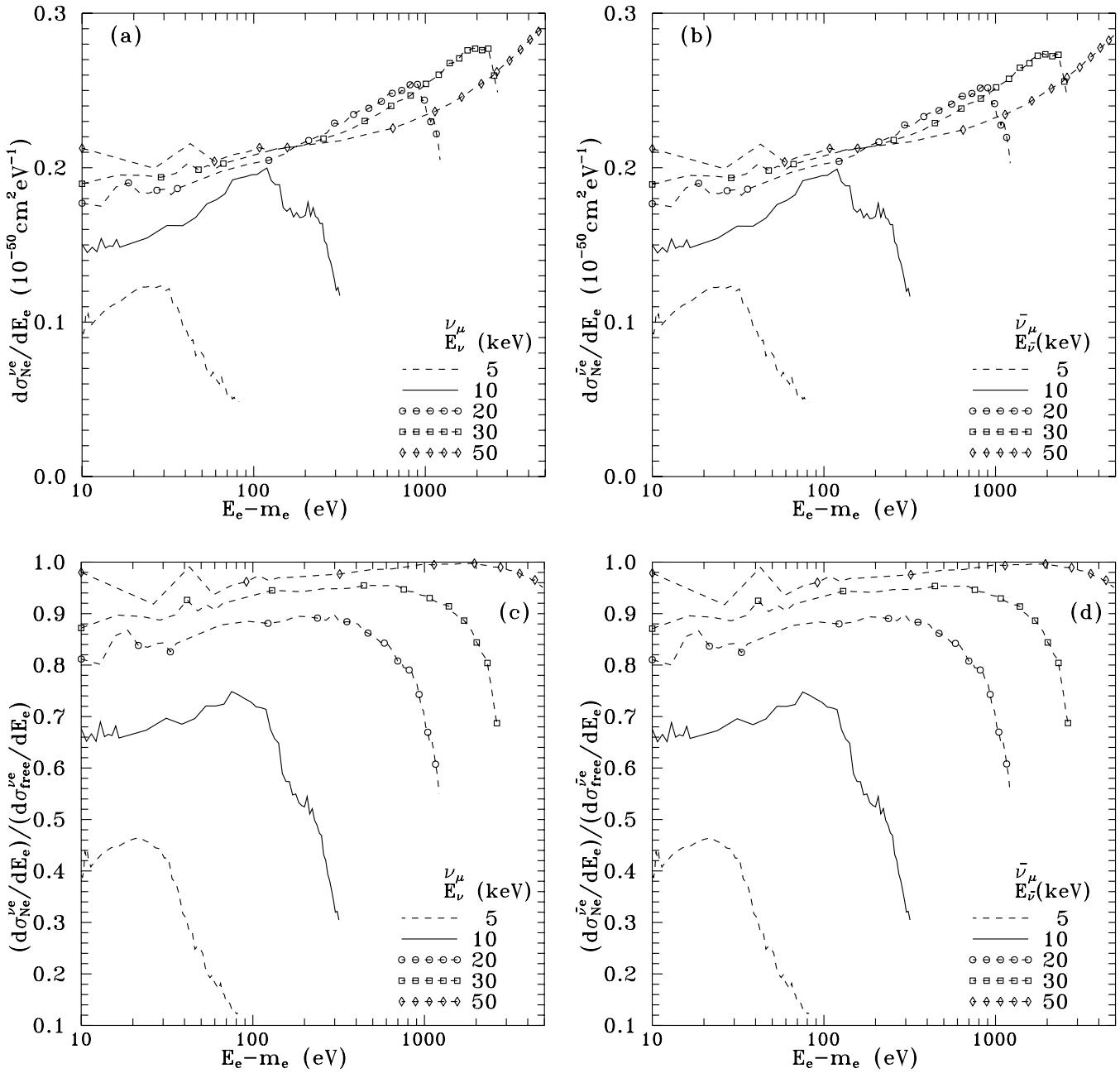

FIG. 8. The electron energy distribution in ν_μ (a) or $\bar\nu_\mu$ (b) ionization of Ne normalized to one e^- per unit volume, and their respective ratios (c) and (d) to the corresponding distributions when the initial electron is assumed as free; see Fig. 7. Identical results for ν_τ

through

$$\tilde R_{nl}(k) = 4\pi \int_0^\infty dr r^2 R_{nl}(r) j_l(kr), \qquad \text{(B3)}$$

where $j_l(kr)$ is a spherical Bessel function. The normalization is such that

$$\int \frac{d^3k}{(2\pi)^3} |\tilde\Psi_{nlm}(\vec k)|^2 = 4\pi \int_0^\infty \frac{k^2 dk}{(2\pi)^3} |\tilde R_{nl}(k)|^2 = 1. \qquad \text{(B4)}$$

We next turn to the explicit form of momentum-wave functions for the ground state of the various atoms. For hydrogen, the standard ground state wave function is

$$\tilde\Psi_{100}(k) = \frac{1}{\sqrt{4\pi}} \tilde R_{10}(k) = \frac{8\sqrt{\pi}(Z_H)^{5/2}}{[k^2 + (Z_H)^2]^2}, \qquad \text{(B5)}$$

with $Z_H = m_e \alpha$ being the inverse Bohr radius of the H atom. In all cases involving integrals over the hydrogen momentum-wave function, we integrated over the range

$0 \leq k \lesssim 3Z_H$, which describes very accurately the relevant momentum range of the bound electron.

For the heavier atoms we follow [11], based on the RHF approach, also explained in [15]. Accordingly, the radial momentum-wave functions are written as

$$\tilde{R}_{nl}(k) = \sum_j C_{jln} \tilde{S}_{jl}(k), \tag{B6}$$

in terms of the RHF functions $\tilde{S}_{jl}(k)$ in momentum space, related to $S_{jl}(r)$ given in Ref. [11] through

$$\tilde{S}_{jl}(k) = 4\pi \int_0^\infty dr r^2 S_{jl}(r) j_l(kr), \tag{B7}$$

in analogy to (B3). Since $S_{jl}(r)$ also depend on a parameter called n_{jl}, tabulated in [11], the corresponding momentum RHF functions are

$$\begin{aligned}
l = 0, \qquad n_{j0} = 1 &\rightarrow \tilde{S}_{j0}(k) = \frac{16\pi Z_{j0}^{5/2}}{(Z_{j0}^2 + k^2)^2}, \\
n_{j0} = 2 &\rightarrow \tilde{S}_{j0}(k) = \frac{16\pi Z_{j0}^{5/2}(3Z_{j0}^2 - k^2)}{\sqrt{3}(Z_{j0}^2 + k^2)^3}, \\
n_{j0} = 3 &\rightarrow \tilde{S}_{j0}(k) = \frac{64\sqrt{10}\pi Z_{j0}^{9/2}(Z_{j0}^2 - k^2)}{5(Z_{j0}^2 + k^2)^4}, \\
n_{j0} = 4 &\rightarrow \tilde{S}_{j0}(k) = \frac{64\pi Z_{j0}^{9/2}(5Z_{j0}^4 - 10Z_{j0}^2 k^2 + k^4)}{\sqrt{35}(Z_{j0}^2 + k^2)^5}, \\
n_{j0} = 5 &\rightarrow \tilde{S}_{j0}(k) = \frac{128\sqrt{14}\pi Z_{j0}^{13/2}(3Z_{j0}^4 - 10Z_{j0}^2 k^2 + 3k^4)}{21(Z_{j0}^2 + k^2)^6},
\end{aligned} \tag{B8}$$

$$\begin{aligned}
l = 1, \qquad n_{j1} = 2 &\rightarrow \tilde{S}_{j1}(k) = \frac{64\pi k Z_{j1}^{7/2}}{\sqrt{3}(Z_{j1}^2 + k^2)^3}, \\
n_{j1} = 3 &\rightarrow \tilde{S}_{j1}(k) = \frac{64\sqrt{10}\pi k Z_{j1}^{7/2}(5Z_{j1}^2 - k^2)}{15(Z_{j1}^2 + k^2)^4}, \\
n_{j1} = 4 &\rightarrow \tilde{S}_{j1}(k) = \frac{128\pi k Z_{j1}^{11/2}(5Z_{j1}^2 - 3k^2)}{\sqrt{35}(Z_{j1}^2 + k^2)^5}, \\
n_{j1} = 5 &\rightarrow \tilde{S}_{j1}(k) = \frac{128\sqrt{14}\pi k Z_{j1}^{11/2}(35Z_{j1}^4 - 42Z_{j1}^2 k^2 + 3k^4)}{105(Z_{j1}^2 + k^2)^6},
\end{aligned} \tag{B9}$$

$$\begin{aligned}
l = 2n_{j2} = 3 &\rightarrow \tilde{S}_{j2}(k) = \frac{128\sqrt{10}\pi k^2 Z_{j2}^{9/2}}{5(Z_{j2}^2 + k^2)^4}, \\
n_{j2} = 4 &\rightarrow \tilde{S}_{j2}(k) = \frac{128\pi k^2 Z_{j2}^{9/2}(7Z_{j2}^2 - k^2)}{\sqrt{35}(Z_{j2}^2 + k^2)^5}.
\end{aligned} \tag{B10}$$

The parameters $(C_{jln}, n_{jl}, Z_{jl})$ appearing in (B6) and (B8)–(B10) are given in the tables in [11]. Parameters (C_{jln}, n_{jl}) are dimensionless, while Z_{jl} are expressed in units of $m_e\alpha = 3.73$ keV in [11].

We also note that, according to (B6) and (B8)–(B10) and [11], the highest Z_{j0} for each atomic state determines the relevant range where the bound electron's momentum mostly lies.[13] In most cases, this range is found to be $0 \leq k \lesssim 3\max(Z_{j0})m_e\alpha$.

[13]Compare (B5) and the related variable Z_H.

[1] H. S. Gurr, F. Reines, and H. W. Sobel, Phys. Rev. Lett. **28**, 1406 (1972); CHOOZ Collaboration, M. Apollonio *et al.*, Phys. Lett. B **446**, 415 (1999); Superkamiokande Collaboration, Y. Fukuda *et al.*, Phys. Rev. Lett. **82**, 2644 (1999); Borexino Collaboration, A. Ianni, Nucl. Phys. **A663**, 791 (2000); J. N. Bahcall, M. C. Gonzalez-Garcia, and C. Peña-Garay, J. High Energy Phys. 08 (2004) 016.

[2] J. Bouchez and I. Giomataris, CEA/Saclay Report No. DAPNIA/01-07, 2001; Y. Giomataris, Ph. Rebourgeard, I. P. Robert, and G. Charpak, Nucl. Instrum. Methods Phys. Res., Sect. A **376**, 29 (1996); J. L. Collar and I. Giomataris, in *Proceedings of the IMAGING 2000 Conference, Stockholm* (Report No. DAPNIA/00-06, 2000).

[3] KamLAND Collaboration, T. Araki *et al.*, hep-ex/0405035.

[4] For a recent review, see, e.g., M. Maltoni, T. Schwetz, M. A. Tortola, and J. W. F. Valle, hep-ph/0405172; G. Sigl, hep-ph/0408165, and references therein.

[5] Y. Giomataris and J. D. Vergados, Nucl. Instrum. Methods Phys. Res., Sect. A **530**, 330 (2004); Y. Giomataris and J. D. Vergados, hep-ph/0311007.

[6] S. A. Fayans, V. Yu. Dobretsov, and A. B. Dobrosvetov, Phys. Lett. B **291**, 1 (1992); V. Y. Dobretsov, A. B. Dobrosvetov, and S. A. Fayans, Sov. J. Nucl. Phys. **55**, 1180 (1992).

[7] G. C. McLaughlin and C. Volpe, Phys. Lett. B **591**, 229 (2004); G. C. McLaughlin and J. N. Ng, Phys. Lett. B **493**, 88 (2000).

[8] O. G. Miranda, V. Semikoz, and J. W. F. Valle, Phys. Rev. D **58**, 013007 (1998).

[9] G. J. Gounaris, E. A. Paschos, and P. I. Porfyriadis, Phys. Lett. B **525**, 63 (2002).

[10] Yu. V. Gaponov, Yu. L. Dobrynin, and V. I. Tikhonov, Sov. J. Nucl. Phys. **22**, 170 (1975).

[11] C. F. Bunge, J. A. Barrientos, and A. V. Bunge, At. Data Nucl. Data Tables **53**, 113 (1993); C. F. Bunge, J. A. Barrientos, A. V. Bunge, and J. A. Cogordan, Phys. Rev. A **46**, 3691 (1992).

[12] The electron binding energies are taken from http://www.webelements.com/webelements/; see also http://www.chembio.uoguelph.ca/educmat/atomdata/bindener/elecbind.htm

[13] Y. Giomataris (private communication).

[14] A. Tubis, Phys. Rev. **102**, 1049 (1956); C. Zener, Phys. Rev. **36**, 51 (1930); P. M. Morse, L. A. Young, and E. S. Haurwitz, Phys. Rev. **48**, 948 (1935).

[15] J. C. Slater, *Quantum Theory of Atomic Structure* (McGraw-Hill Book Company, NY, 1960), Vol. I.